High Bandgap Perovskites for Efficient Indoor Light Harvesting

Sergey Shcherbachenko[1,2], Oleksandr Astakhov[1], Zhifa Liu[1], Li-Chung Kin[1,3], Christoph Zahren[1], Uwe Rau[1,2], Thomas Kirchartz[1,4], Tsvetelina Merdzhanova[1]*

[1]IEK-5 Photovoltaik, Forschungszentrum Jülich GmbH, Wilhelm-Johnen Straße, 52425 Jülich, Germany

[2]Jülich Aachen Research Alliance, JARA-Energy and Faculty of Electrical Engineering and Information Technology, RWTH Aachen University, Schinkelstr. 2, 52062 Aachen, Germany

[3]IEK-9, Grundlagen der Elektrochemie, Forschungszentrum Jülich, 52425 Jülich, Germany

[4]Faculty of Engineering and CENIDE, University of Duisburg-Essen, Carl-Benz-Str. 199, 47057 Duisburg, Germany

*Email: t.merdzhanova@fz-juelich.de

ABSTRACT

The use of metal-halide perovskites in photovoltaic applications has become increasingly attractive owing to their low-temperature manufacturing processes and long charge-carrier lifetimes. High-bandgap perovskite solar cells have potential for indoor applications owing to their efficient absorption of the LED spectrum. This study investigates the performance of high-bandgap perovskite solar cells under a wide range of lighting conditions, including a commercially available white LED lamp with a 5 – 40000 lx illuminance range and a standard 1 sun reference. We compare the performance of $CH_3NH_3PbI_3$ based perovskite solar cells to $CH_3NH_3Pb(I_{0.8,}Br_{0.2})_3$ solar cells with varying electron transport layers (ETL), including PCBM, PCBM:CMC, and CMC:ICBA fullerene combinations. Because the spectral response of perovskite solar cells covers the white LED spectrum very well, the major performance difference is related to the open-circuit voltage and fill factor (V_{OC} and *FF*). The cells with the $CH_3NH_3Pb(I_{0.8,}Br_{0.2})_3$ absorber layer and the CMC:ICBA electron transport layer demonstrate superior open-circuit voltage and therefore a high efficiency above 29% at 200 – 500 lx, typical for indoor lighting.

INTRODUCTION

Low-temperature manufacturing processes using inexpensive solution-processing methods [1], combined with exceptionally long charge-carrier lifetimes [2-4] have made metal-halide perovskites attractive materials for photovoltaic applications. [5] Owing to intensive research efforts, efficiencies have increased to 25.7% [6] over the course of 10 years, since the

first cells surpassed the 10% mark in 2012. [7] A peculiar feature of halide perovskites is that they achieve their best efficiencies for bandgaps that are slightly higher than ideal from the perspective of the Shockley-Queisser model for the sunlight spectrum. [8, 9] This has led to a continuously increasing interest in using halide perovskites for tandem solar cells [10-12] but also offers opportunities to employ the technology for artificial lighting conditions. [13] As the future of lighting is in white LEDs, and because white LEDs have significantly fewer infrared (IR) and near-infrared spectral components as compared to traditional light bulbs or the solar spectrum, higher bandgap materials are needed for maximum efficiencies. Depending on the spectrum and color temperature of the LEDs used, the optimum bandgaps for indoor applications range from around 1.7 eV to 2 eV. [14] These bandgaps are significantly higher than those of crystalline silicon (1.12 eV) and even those of the halide perovskite solar cells (1.5 to 1.6 eV) that show the best efficiencies under one-Sun illumination. [15] Thus, there is a need to explore perovskite solar cells with higher bandgaps (> 1.7 eV). Perovskite technology provides sufficient flexibility to fabricate these solar cells. However, high-bandgap perovskite cells often suffer from effects such as iodine-bromine segregation, [16, 17] increased bulk recombination [18], and a lack of suitable charge transport materials with good energy level matching at interfaces. [19-22]

Artificial indoor LED lighting is characterized by a narrower spectrum and significantly reduced intensity with respect to the one-Sun standard test conditions. A drastic decrease in intensity leads to an efficiency reduction [23-26]. At low illumination, even a low current through the parasitic shunt resistance gains importance and reduces solar cell efficiency. [23, 25-27] Perovskite solar cells, however, show potential for a high shunt resistance R_{SH}, [13, 28-31] making them suitable for low-illumination applications. In addition, Kin et al. demonstrated the exceptional efficiency of these cells when integrated with sodium-ion batteries under indoor illumination. [32]

Spectrum narrowing can be very beneficial for solar cell efficiency. [13, 14, 23, 28-31, 33] The emission spectra of indoor LED light sources are often very efficiently absorbed by the perovskite solar cells and, therefore, the losses in short-circuit current density J_{SC} are low. Therefore, most optimization efforts must focus on the V_{OC} and *FF* losses under indoor illumination. In this work, we focus on maximizing the V_{OC} of the perovskite solar cells for indoor applications.

To explore this optimization direction, we studied the light intensity dependent performance of $CH_3NH_3Pb(I,Br)_3$ solar cells with different I to Br ratios that have fairly high open-circuit

voltages between 1.19 and 1.33 V for bandgaps between 1.6 and 1.72 eV. We compare two absorber compositions with (i) pure iodine ($CH_3NH_3PbI_3$, E_g = 1.6 eV) and with 20% Br ($CH_3NH_3Pb(I_{0.8,}Br_{0.2})_3$, E_g = 1.72 eV). The absorbers were grown using $PbAc_2$-based precursors, as previously described by Liu et al. [19, 34] The solar cells are based on a pin-type geometry, as shown in Figure 1, where the perovskite layer is sandwiched between an ITO/PTAA anode on the illuminated front side of the device and a fullerene / bathocuproine (BCP)/Ag cathode on the back. The fullerenes employed include [6,6]-phenyl-C_{61}-butyric acid methyl ester (PCBM), which is used for Br-free cells, and PCBM, PCBM:CMC, and CMC:ICBA for Br-containing cells. Here, ICBA is the indene-C_{60} bisadduct known for its significantly lower electron affinity [35, 36] as compared to PCBM or even C_{60}, whereas CMC is C_{60}-fused N-methylpyrrolidine-m-C_{12}-phenyl. The use of lower electron affinity fullerenes, such as ICBA and CMC, is crucial for improving the energy-level alignment to higher bandgap perovskites and minimizing losses due to interfacial recombination, which are known to deteriorate the performance of high-bandgap perovskite solar cells. Both absorber compositions have been previously shown to enable high open-circuit voltages [19, 34] owing to their very high bulk lifetimes, negligible recombination at the perovskite-PTAA interface, and reduced recombination at the perovskite-ETL interface. However, it has already been clear from previous work that the perovskite-ETL interface is the performance-limiting interface that causes significant additional recombination in the device compared to perovskite films on glass or on PTAA. [2, 37] In this work, we vary the ETL layer between the combinations of PCBM, CMC, and ICBA fullerenes and study the performance of these cells under LED illumination with varied irradiance and under 1 Sun illumination. Following our previous work[19, 34] dedicated to achieving high 1 Sun V_{OC} in these cells, we now focus on performance under LED light and discuss trends in irradiance dependence that affect the indoor light harvesting performance.

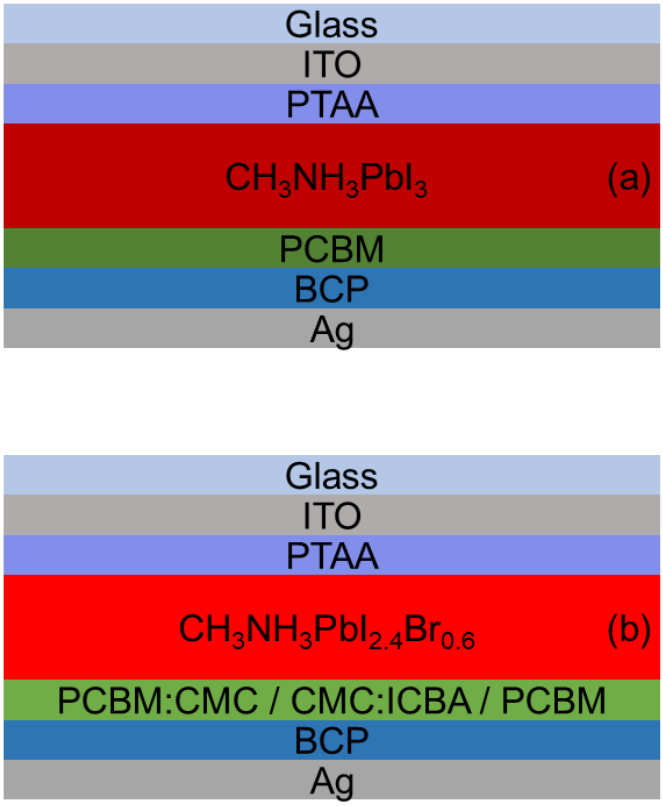

Figure 1 Schematic of the layer stacks of the perovskite solar cells used in this study. The solar cell with the $CH_3NH_3PbI_3$ absorber layer (a) has a PCBM electron transport layer (ETL). Solar cells with the $CH_3NH_3Pb(I_{0.8},Br_{0.2})_3$ absorber layer (b) have electron-transport layers consisting of different combinations of the fullerenes PCBM, CMC, and ICBA.

RESULTS AND DISCUSSION

Four types of perovskite solar cells were investigated in this work: high-bandgap $CH_3NH_3Pb(I_{0.8},Br_{0.2})_3$ cells with CMC:ICBA, PCBM and PCBM:CMC electron-transport layers and a reference $CH_3NH_3PbI_3$ cell with a PCBM electron transport layer. The fabrication procedure for the $CH_3NH_3PbI_3$ cell was discussed in ref. [34], while the detailed fabrication procedure for the $CH_3NH_3Pb(I_{0.8},Br_{0.2})_3$ cells was presented in ref. [19]. Figure **2** presents the *JV*-curves of these solar cells under 1 Sun and 175 lx LED illumination (lowest measured point close to the 200 – 500 lx region).

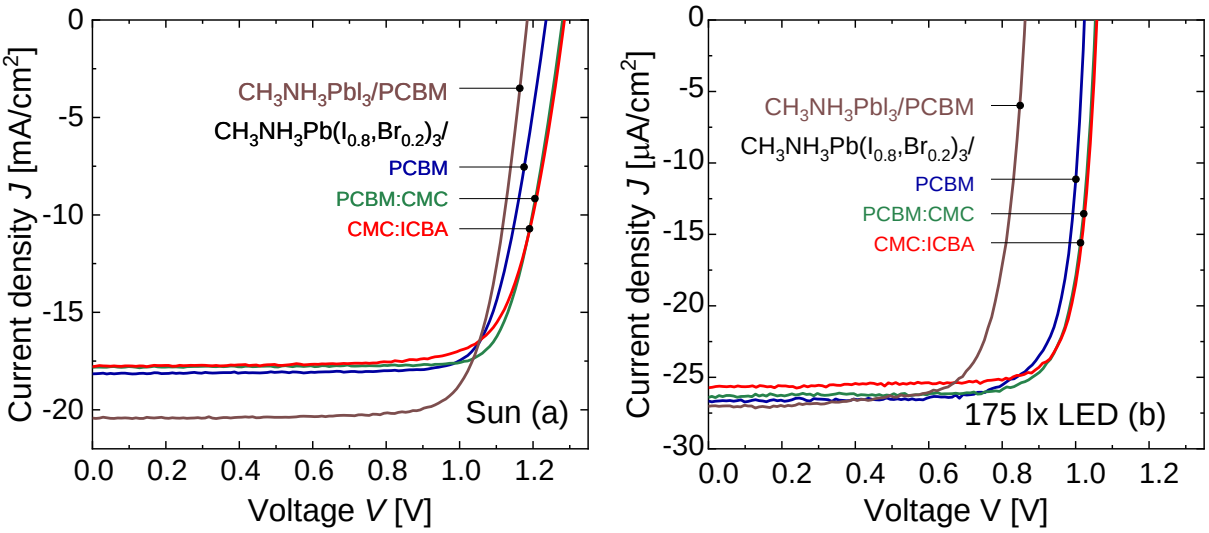

Figure 2 *JV*-characteristics of PSCs used in this study under 1 Sun (a) and 175 lx LED light (b). The solar cell with the $CH_3NH_3PbI_3$ absorber layer has a PCBM electron-transport layer. Three solar cells with a $CH_3NH_3Pb(I_{0.8},Br_{0.2})_3$ absorber layer have PCBM, PCBM:CMC and CMC:ICBA fullerene blends as electron-transport layers (ETL).

Table **1** presents the corresponding solar cell parameters: open-circuit voltage (V_{OC}), short-circuit current (I_{SC}), short-circuit current density (J_{SC}), short-circuit current density calculated from EQE ($J_{SC,\ EQE}$), device area (A), fill factor (FF), power at maximum-power point (P_{MPP}) and efficiency (η). $J_{SC,\ EQE}$ was calculated for two cells (with $CH_3NH_3Pb(I_{0.8},Br_{0.2})_3$ absorber and CMC:ICBC electron transport layers and with $CH_3NH_3PbI_3$ absorber and PCBM electron transport layers) using EQE measured for the cells with the same composition.

Table 1 Parameters of perovskite solar cells used in this study under room conditions (175 lx LED) and under 1 Sun.

	$CH_3NH_3Pb(I_{0.8},Br_{0.2})_3$		$CH_3NH_3Pb(I_{0.8},Br_{0.2})_3$		$CH_3NH_3Pb(I_{0.8},Br_{0.2})_3$		$CH_3NH_3PbI_3$	
	CMC:ICBA		PCBM:CMC		PCBM		PCBM	
Source	LED	Sun	LED	Sun	LED	Sun	LED	Sun
V_{OC} [V]	1.06	1.29	1.05	1.28	1.02	1.24	0.86	1.18
I_{SC} [mA]	0.0041	2.85	0.0042	2.85	0.0043	2.90	0.0043	3.27
J_{SC} [mA/cm²]	0.0257	17.79	0.0264	17.82	0.0267	18.15	0.0270	20.43
$J_{SC,\ EQE}$ [mA/cm²]	0.02560	18.68	-	-	-	-	0.0288	20.04
A [cm²]	0.16	0.16	0.16	0.16	0.16	0.16	0.16	0.16
FF [%]	80.82	75.87	79.86	79.58	77.97	78.22	74.11	77.65
P_{MPP} [mW/cm²]	0.0220	17.30	0.0222	18.20	0.0213	17.50	0.0173	18.80
η [%]	29.36	17.30	29.62	18.20	28.42	17.50	23.09	18.80

The solar cell with the $CH_3NH_3PbI_3$ absorber layer has a bandgap of 1.6 eV and consequently lower V_{OC} of 0.86 V at 175 lx LED and 1.18 V at 1 Sun. PSCs with the $CH_3NH_3Pb(I_{0.8},Br_{0.2})_3$ (1.72 eV bandgap) absorber layer show open-circuit voltages in the range of 1.24 – 1.3 V at 1 Sun and around 1.02 – 1.06 V at 175 lx LED illumination. Among them, the cell with a blend of CMC and ICBA used as an electron-transport layer has the highest V_{OC} of 1.29 V at 1 Sun and 1.06 V at 175 lx LED illumination. From the low illumination current – voltage curves (Figure **2**b), one can see that the shunt resistance of these cells is extremely high, ensuring a stable and high *FF* (above 75% for CMC:ICBA electron transport layer cells) even at 175 lx. Although in this work $CH_3NH_3PbI_3$ cells show considerably lower voltages than $CH_3NH_3Pb(I_{0.8},Br_{0.2})_3$ cells, our previous work on this cell reported an even higher V_{OC} of 1.26 V after light soaking. [34]

Figure **3** (a, b) presents the open-circuit voltage V_{OC} and fill factor dependences on the light source power density for the solar cells used in this study.

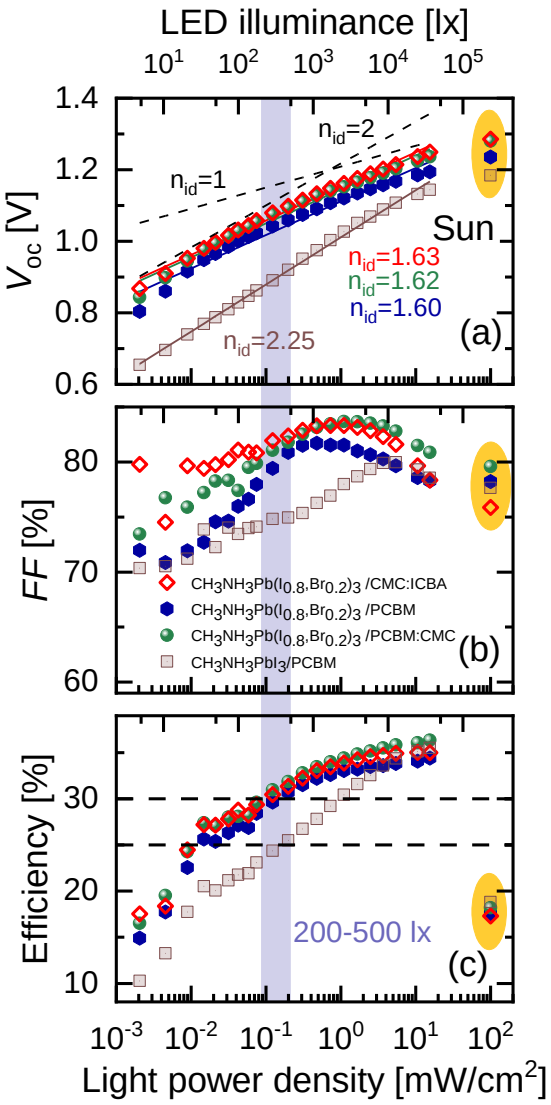

Figure 3 Open circuit voltage, V_{OC} (a), fill factor, *FF* (b) and power conversion efficiency (c) as a function of the power density of the LED and reference values measured under 1 Sun illumination (yellow area) for different perovskite solar cells. The top x-axis corresponds to illuminance values in lux calculated for the LED spectrum (1 Sun AM1.5 spectrum corresponds to 100 mW/cm^2 and approximately 10^5 lx, and the position of the points is defined by the power density value). The region marked with blue rectangle represents standard office room conditions (200 – 500 lx). The ideality factors of the three wide-band-gap perovskites are labelled in (a) in their corresponding colors.

The measurement results under standard test conditions, 1 Sun illumination are highlighted in yellow. The region of typical indoor illumination (200 – 500 lx) is marked by a blue vertical bar in Figure **3**. The LED power density range of all points tested is 0.002 – 15.5 mW/cm^2 and corresponds to approximately 5 – 40000 lx.

For all perovskite solar cells (PSCs) a smooth quasi-linear dependence of V_{OC} on power density is observed on the semi-logarithmic scale. The cells closely follow the classical diode dependence of V_{OC} on J_{SC} [38, 39]

$$V_{OC} = \frac{n_{id}kT}{q} ln\left(\frac{Jsc}{J_0}\right). \quad [1]$$

Using equation **1**, the ideality factors of these cells were determined from the data in Figure **3**a. The dashed lines representing the slopes for $n_{id} = 1$ and $n_{id} = 2$ are plotted for reference. The solar cells with $CH_3NH_3Pb(I_{0.8,}Br_{0.2})_3$ showed ideality factors between 1.6 and 1.63, while the lower bandgap $CH_3NH_3PbI_3$ cell showed an ideality factor of 2.25. A lower ideality factor corresponds to a flatter slope and a higher V_{OC} at low irradiance. The higher-bandgap cells in this study showed considerably more stable V_{OC} over the entire illuminance range compared to the cell with a lower bandgap. The V_{OC} decreases by approximately 0.38 V in high-bandgap cells as the illuminance decreases from 40000 to 5 lx, while a larger V_{OC} reduction of 0.49 V is observed in the lower-bandgap solar cell. Simultaneously, similar V_{OC} values are observed for 1 Sun illumination and high-power LED illumination. Higher initial voltages of the $CH_3NH_3Pb(I_{0.8,}Br_{0.2})_3$ cells (Figure **3**a) combined with lower V_{OC} drops result in higher *V*oc values at low irradiance as compared to a perovskite solar cell with a $CH_3NH_3PbI_3$ absorber layer (brown squares in Figure **3**a). Under indoor illumination conditions, the $CH_3NH_3Pb(I_{0.8,}Br_{0.2})_3$ cell with the CMC:ICBA electron-transport layer (red diamonds) shows a V_{OC} above 1.05V and we observe a strong difference between low-bandgap and high-bandgap solar cells. $V_{OC} = \frac{n_{id}kT}{q} ln\left(\frac{Jsc}{J_0}\right)$. [*1*

A special note can be given to the V_{OC} of the CMC:ICBA cell. The V_{OC} of this device remained above 1.1 V under LED illumination with an irradiance of 0.3 mW/cm^2 and increased up to 1.3 V at 15.5 mW/cm^2. Under 1 Sun illumination (100 mW/cm^2 AM1.5), the cell showed a V_{OC} of 1.29 V. These results are in agreement with those of our previous work [19], where the highest voltage was achieved by a cell with the same structure.

The fill factor (*FF*) of a solar cell *JV* curve is defined as $FF = V_{MPP}\, J_{MPP} / (V_{OC}\, J_{SC})$, where V_{MPP} and J_{MPP} are the voltage and current density at the maximum power point. It depends on the ideality factor n_{id}, as well as the shunt and series resistances R_{SH} and R_S, and is positively correlated with the open-circuit voltage (V_{OC}). Following the approach [40] for the case of an ideal diode with infinitely large shunt resistance and zero series resistance, the *FF* dependence on V_{OC} can be approximated with

$$FF_0 = \frac{v_{oc} - ln(v_{oc} + 0.72)}{v_{oc} + 1}, \quad [2]$$

where

$$v_{oc} = \frac{V_{OC}}{nkT/q}. \quad [3]$$

As the V_{OC} increases with the illumination intensity (Figure **3**a), an increase in *FF* is observed (Figure **3**b) for all perovskite solar cells. Additionally, the *FF* strongly depends on the shunt and series resistances of the solar cell [41, 42]. The effect of the shunt resistance is more pronounced under low LED light power density, whereas the series resistance is important at high illumination intensities, where the current density at the maximum power point increases [26]. The series resistance of the cells leads to a drop in the *FF* observed under LED irradiance above 10000 lx. At the same time, perovskite solar cells can have a remarkably high shunt resistance, [13, 28-31] which was also the case for the presented PSCs (Figure ***4***), demonstrating a very stable *FF* at low illumination intensities.

Figure **3**c presents the dependence of the cell efficiency on the LED power density and includes the reference values under one-sun irradiance represented by the points in the yellow area. Comparing the performance of perovskite solar cells under one-Sun and under high power densities of white LED, higher power conversion efficiencies were observed under LED light (34 – 36.5% under LED vs 17 – 19% under 1 Sun). This is related to the high-bandgap of the perovskite absorbers and, therefore, a much better match of their EQE to the LED spectrum as compared to the Sun spectrum (see Figure **6**). In the case of LED light, both perovskite absorber materials show external quantum efficiencies above 80% over the entire range of the LED spectrum, except for the minor fraction of the IR region 740 – 800 nm, where the LED emission

is weak. Therefore, under LED light, both absorbers exhibited very similar J_{SC} values (Table 1). At the same time, the wider bandgap of $CH_3NH_3Pb(I_{0.8},Br_{0.2})_3$ provides a noticeably higher V_{OC}, likely due to the reduction in thermalization losses even under LED light. The thermalization loss refers to the energy loss during vibrational (thermal) relaxation of an excited electron to the lowest available level of the conduction band [43]. A high bandgap reduces the amount of energy that an electron releases during such a process and results in a considerably higher V_{OC} and efficiency of the cells with the $CH_3NH_3Pb(I_{0.8},Br_{0.2})_3$ base layer. The cell with the highest V_{OC} has a CMC:ICBA ETL layer and shows an efficiency of above 29% in office-lighting conditions (200-500 lux), 28.5% efficiency under a lower illuminance of 100 lx, while a maximum efficiency of 35.5% is observed under approximately 4000 lx of LED light.

Figure ***4***a presents the dependence of the shunt resistance (R_{SH}) on the LED light power density.

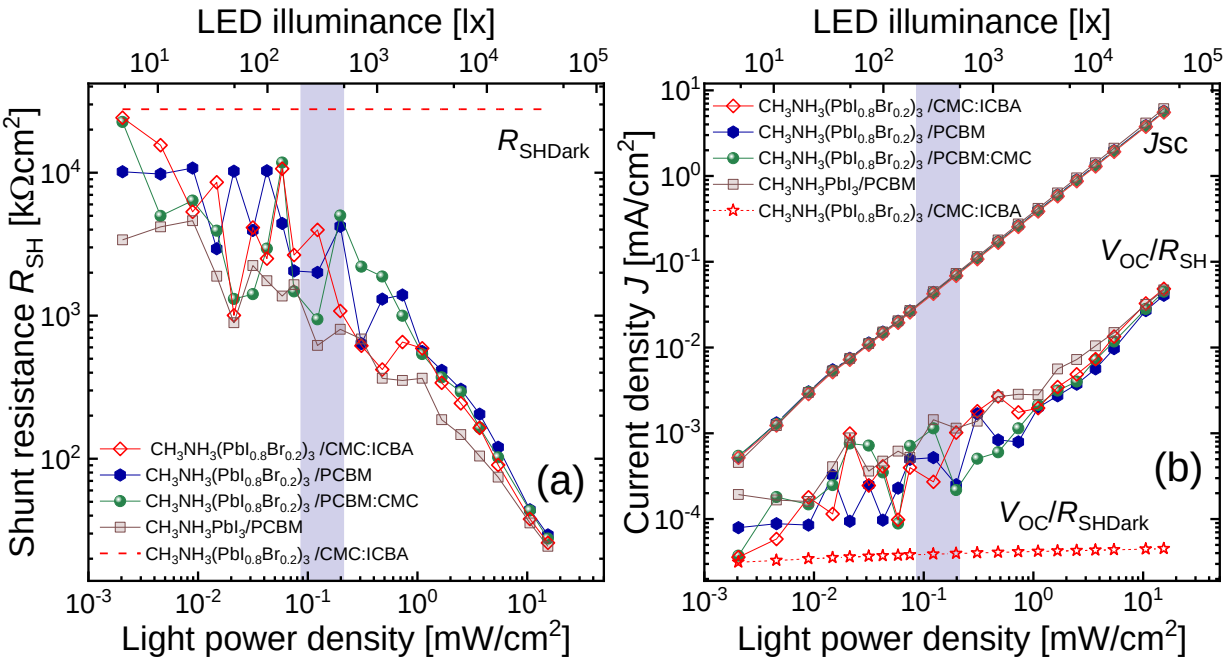

Figure 4 Dependence of the shunt resistance R_{SH} (a) on LED light power density for different perovskite solar cells. Dependence of the short-circuit current density and the estimated shunt current (calculated as V_{OC}/R_{SH}) on LED light power density (b). The top x-axis corresponds to illuminance values in lux. The values of R_{SH} and V_{OC}/R_{SH} with R_{SH} calculated from the dark JV (R_{SHDark}) are presented for one cell as a reference in both plots (red dashed line(a) and red stars(b)). The region marked with blue rectangle represents standard office room conditions (200 – 500 lx).

The resistance was determined from the slope of the corresponding *JV* curve at $V = 0$, so any linear term in the dependence of current on voltage was perceived as shunt. As a result, we observe the real shunt resistance in parallel with a "photo-shunt" [44, 45], which shows a linear dependence on the light power density. As these two effects act in parallel, the lower of the two resistances will dominate. At high LED power density, the photo-shunt resistance decreases, and the overall resistance shows a linear dependence on light intensity. Moving to low irradiance, the photo-shunt resistance increases, while the total shunt resistance saturates around the value determined from the dark *JV* curve (~20000 kΩcm^2). In the region corresponding to room conditions (marked with blue rectangle) perovskite solar cells show shunt resistances above 1000 kΩcm^2.

In the single diode model with shunt resistance, a correction term V_{OC}/R_{SH} appears (Equation 4**),** which leads to the reduction of V_{OC}.

$$V_{OC} = \frac{n_{id}kT}{q} \ln\left(\frac{J_{SC} - V_{OC}/R_{SH}}{J_0}\right). \quad [4]$$

The value of this correction term V_{OC}/R_{SH} is compared to the magnitude of J_{SC} in Figure 4b for the studied LED power density range. As the J_{SC} is at least one (almost two) order of magnitude higher than V_{OC}/R_{SH} at irradiances corresponding to room conditions and above, the shunt resistance has minor influence on the V_{OC} in the Perovskite cells presented in this study.

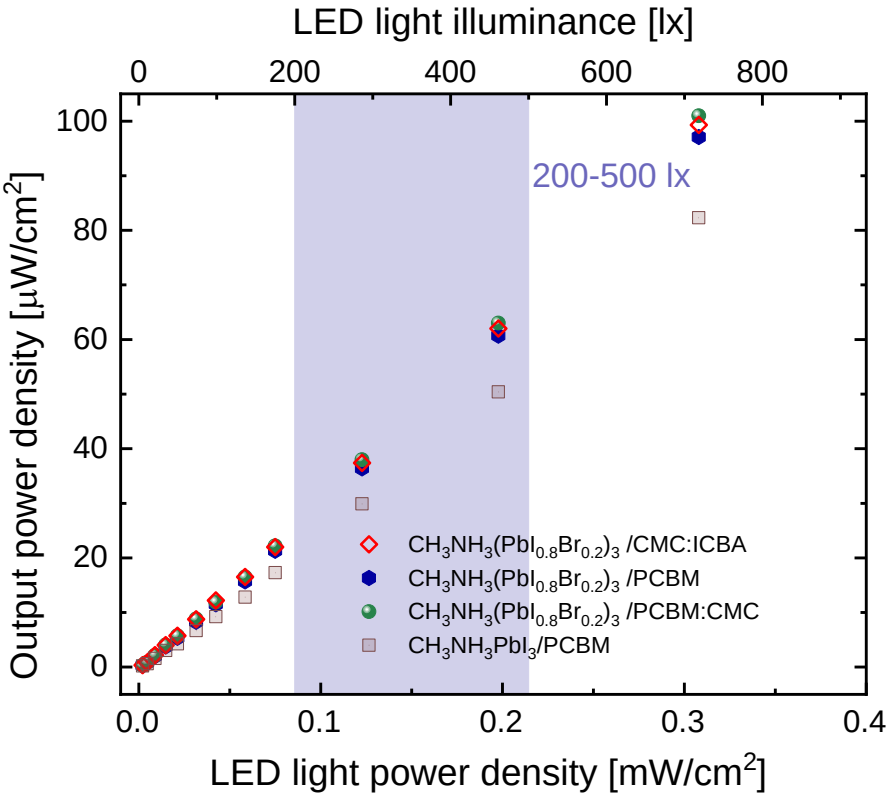

Figure 5 Dependence of the output power density of PSCs on the power density delivered by the LED light source. The blue region represents standard office room conditions (200 – 500 lx).

The dependencies presented in Figure 3 fully describe the performance of the studied cells, but for potential practical indoor applications of PSCs, it is more instructive to plot the dependence of the PSC output power density on the LED lighting power density on a linear scale as it is presented in Figure **5**. For example, the PSCs used in this study can provide a power density of 38 μW/cm^2 under LED illumination with 0.12 mW/cm^2 power density. Additionally, a power density of 20 – 60 μW/cm^2 can be expected in suggested room lighting conditions (white LED illumination of 200 – 500 lx). This value can be used to estimate the solar cell (or module) area required to supply power to certain electronic applications in an indoor setting.

Table 2 Comparison of the performance between the $CH_3NH_3Pb(I_{0.8},Br_{0.2})_3$ cell with CMC:ICBA electron transport layer and other reported perovskite cells in similar conditions.

Irradiance	Illuminance of LED	Cell efficiency	Reference	This work
$0.3 mW/cm^2$	800 lx	40.1%	[13]	32.3%
--	1000 lx	36.2%	[29]	32.6%
$0.3 mW/cm^2$	1000 lx	27.4%	[31]	32.6%
--	400 lx	26.9%	[28]	30.9%
--	200 lx	25%	[30]	29.4%
--	100 lx	22.5%	[31]	28.5%

Comparing the results of this work with the literature data [13, 28-31] we conclude that the PSC with the $CH_3NH_3Pb(I_{0.8},Br_{0.2})_3$ bandgap and CMC:ICBA has exceptionally good performance under white LED illumination of 100-1000 lx (Table 2) and stays on par with or exceeds the best values reported in the literature, especially in the relevant for indoor application range of 200-500 lx [13, 28-31].

CONCLUSIONS

We studied the potential of high-bandgap perovskite solar cells (PSCs) for indoor applications under LED light. The quantum efficiency of PSCs closely matches that of common LED lights, thereby providing efficient absorption. Therefore, further performance improvement efforts must focus on V_{OC} and *FF* under low-intensity LED light. To achieve a high V_{OC} under low-light conditions, we studied PSCs with a wide-bandgap $CH_3NH_3Pb(I_{0.8},Br_{0.2})_3$ absorber layer (E_g = 1.72 eV) in combination with three electron-transport layers (PCBM) and two PCBM:CMC and CMC:ICBA fullerene combinations. The high-bandgap cells were compared to a reference cell with a $CH_3NH_3PbI_3$ absorber layer (E_g = 1.6 eV) and a PCBM electron transport layer. The wide bandgap $CH_3NH_3Pb(I_{0.8},Br_{0.2})_3$ solar cells showed 1 Sun V_{OC} of 1.24 – 1.29 V, while $CH_3NH_3PbI_3$ solar cell showed lower 1 Sun V_{OC} of 1.18 V.

All solar cells were tested under LED illumination with illuminance ranging from 5 lx to 40000 lx. The wide-bandgap $CH_3NH_3Pb(I_{0.8},Br_{0.2})_3$ cells reveal persistent V_{OC} with flat dependence on irradiance corresponding to an ideality factor of approximately 1.6 and a V_{OC}

of 1 V around 200 – 500 lx. The reference $CH_3NH_3PbI_3$ cell showed a V_{OC} of 0.86 V at 200 – 500 lx and a steeper V_{OC} dependence on irradiance with ideality factor of approx. 2.25. All studied cells show high FF under low light due to high shunt resistance above 1000 $k\Omega cm^2$. However, the wide bandgap cells demonstrate a higher *FF* in most cases with a *FF* of approx. 80% at 200 – 500 lx. With similar currents but higher V_{OC} and *FF* values, the wide-bandgap cells show a significant gain in efficiency as compared to the reference $CH_3NH_3PbI_3$ cell. Efficiencies of 30 – 32% are observed in the range of 200 – 500 lx, dropping to 28.5% at 100 lx for the highest V_{OC} cell with a $CH_3NH_3Pb(I_{0.8,}Br_{0.2})_3$ absorber layer and a CMC:ICBA electron transport layer. These results agree with the performance of the best reported perovskite solar cells under white LED illumination [13, 28-31] and demonstrate the high potential of the PCSs for indoor light harvesting. To facilitate the practical use of these devices, we present the dependence of the output power density on LED light power density. We expect that light harvesters based on PCSs will deliver approximately 20 – 60 $\mu W/cm^2$ under realistic room lighting conditions.

EXPERIMENTAL

While standards for low-light LED characterization of solar cells are yet to be developed, there are several light conditions that one can usually see in the literature. The region of 300 – 500 lx of "white LED" is a standard for office work.[46] Jobs involving small objects require higher illuminance, whereas offices and non-working areas can have lower average illumination levels [47]. Consequently, the test conditions used in the literature vary between 100 and 1000 lx. At the same time, the standards for illuminance are defined for working desks, while light-harvesting devices can be installed anywhere in a room. Hence, a real room can provide an even wider range of conditions including shaded areas with extremely low illumination. For example, the DIN EN 12464-1 standard sets minimal illuminance of 30 – 50 lx on ceilings and 50 – 75 lx on walls. This paper addresses the performance of perovskite solar cells in a wide range of possible conditions from 5 to 40000 lx, while extending the standard range of office conditions to the 200 – 500 lx range.

Characterization of solar cells under 1 Sun illumination (AM1.5 spectrum, 100 $mWcm^{-2}$) was performed using a class-A sun simulator. A commercially available white LED lamp (Cree XLamp CXA3050 LED with a color temperature of 3000 K) in combination with a neutral-density OD1 filter served as the light source for indoor illumination tests. The standard test procedure involves measurements at different LED light powers, progressing from the lowest

to highest power. We chose this progression to avoid possible light soaking [48, 49] and the influence of the measurements performed at high intensity on the measurements at low intensity. For current−voltage characterization, both forward and backward voltage sweeps were done with 0.01 V steps, 20 ms delay and LED light remaining between the sweeps and changes in irradiance. All presented results correspond to the down-sweep (V_{OC} → J_{SC}) direction.

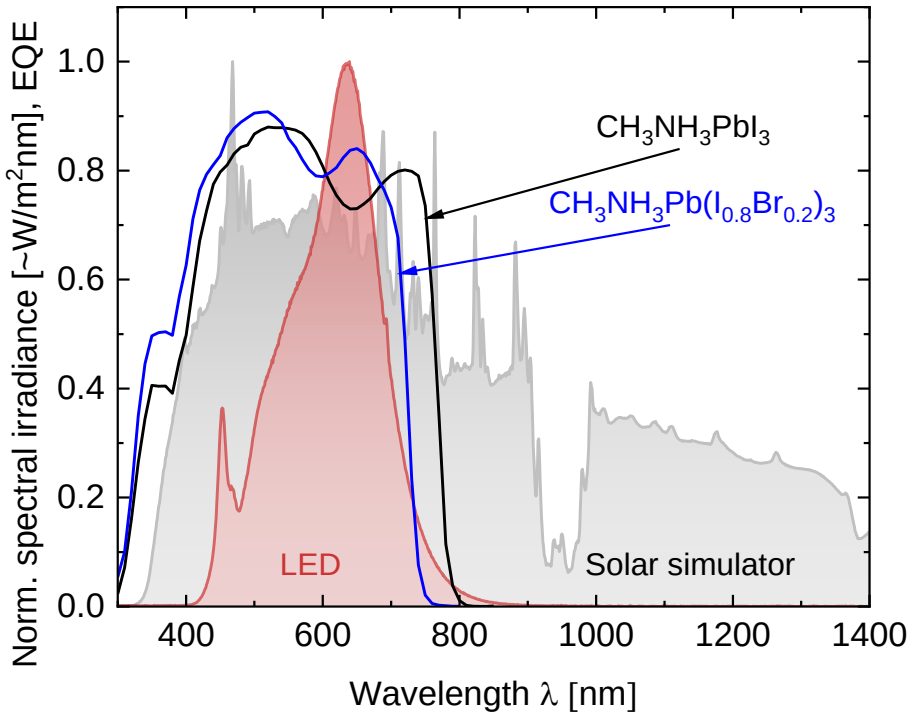

Figure 6 Normalized spectral irradiance of the solar simulator (gray area) and the white LED lamp (red area) used in this study. The spectra are compared with the external quantum efficiencies of $CH_3NH_3PbI_3$ (black line) and $CH_3NH_3Pb(I_{0.8},Br_{0.2})_3$ (blue line) perovskite solar cells.

The power output of the LED lamp was controlled by the LED lamp current. Solar and LED spectra were measured with a compact array spectrometer from "Instrument Systems" at a predefined set of currents. One of the resulting normalized spectra is presented in Figure **6**. From these measurements, the dependence of the irradiance E_e on the LED current was determined and used to interpolate points that were not measured. The spectral response of the neutral-density filter was calculated separately and multiplied by the measured LED spectrum. The illuminance E_v of the LED lamp was calculated from the spectrum of the LED lamp with a filter at a certain LED current and is derived as $E_{v1} = E_{v0} * E_{e1} / E_{e0}$, where E_e is the power density for all other measurement points.

NOTES

The authors declare no conflict of interest.

The data supporting the findings of this study are available from the corresponding author, Tsvetelina Merdzhanova, upon reasonable request.

ACKNOWLEDGEMENTS

The authors would like to thank Benjamin Klingebiel for his help with the measurement box operation. The authors acknowledge the HITEC fellowship program for funding.
This work was supported by the European Union's Horizon Europe as a part of SUPERVAL project (The SUstainable Photo-ElectRochemical VALorization of flue gases) [Grant Agreement No. 101115456].

REFERENCES

[1] Y. Rong, Y. Hu, A. Mei, H. Tan, M. I. Saidaminov, S. I. Seok, M. D. McGehee, E. H. Sargent, H. Han, Science 2018, 361, eaat8235.

[2] L. Krückemeier, B. Krogmeier, Z. Liu, U. Rau, T. Kirchartz, Advanced Energy Materials 2021, 11, 2003489.

[3] D. W. deQuilettes, S. Koch, S. Burke, R. K. Paranji, A. J. Shropshire, M. E. Ziffer, D. S. Ginger, ACS Energy Letters 2016, 1, 438.

[4] W. Tress, Advanced Energy Materials 2017, 7, 1602358.

[5] A. K. Jena, A. Kulkarni, T. Miyasaka, Chemical Reviews 2019, 119, 3036.

[6] O. Almora, D. Baran, G. C. Bazan, C. Berger, C. I. Cabrera, K. R. Catchpole, S. Erten-Ela, F. Guo, J. Hauch, A. W. Y. Ho-Baillie, T. J. Jacobsson, R. A. J. Janssen, T. Kirchartz, N. Kopidakis, Y. Li, M. A. Loi, R. R. Lunt, X. Mathew, M. D. McGehee, J. Min, D. B. Mitzi, M. K. Nazeeruddin, J. Nelson, A. F. Nogueira, U. W. Paetzold, N.-G. Park, B. P. Rand, U. Rau, H. J. Snaith, E. Unger, L. Vaillant-Roca, H.-L. Yip, C. J. Brabec, Advanced Energy Materials 2021, 11, 2102526.

[7] M. M. Lee, J. Teuscher, T. Miyasaka, T. N. Murakami, H. J. Snaith, Science 2012, 338, 643.

[8] W. Shockley, H. J. Queisser, J. Appl. Phys 1961, 32, 510.

[9] L. Krückemeier, U. Rau, M. Stolterfoht, T. Kirchartz, Advanced Energy Materials 2020, 10, 1902573.

[10] K. O. Brinkmann, T. Becker, F. Zimmermann, C. Kreusel, T. Gahlmann, M. Theisen, T. Haeger, S. Olthof, C. Tückmantel, M. Günster, T. Maschwitz, F. Göbelsmann, C. Koch, D. Hertel, P. Caprioglio, F. Peña-Camargo, L. Perdigón-Toro, A. Al-Ashouri, L. Merten, A. Hinderhofer, L. Gomell, S. Zhang, F. Schreiber, S. Albrecht, K. Meerholz, D. Neher, M. Stolterfoht, T. Riedl, Nature 2022, 604, 280.

[11] A. Al-Ashouri, E. Köhnen, B. Li, A. Magomedov, H. Hempel, P. Caprioglio, J. A. Márquez, A. B. Morales Vilches, E. Kasparavicius, J. A. Smith, N. Phung, D. Menzel, M. Grischek, L. Kegelmann, D. Skroblin, C. Gollwitzer, T. Malinauskas, M. Jošt, G. Matič, B. Rech, R. Schlatmann, M. Topič, L. Korte, A. Abate, B. Stannowski, D. Neher, M. Stolterfoht, T. Unold, V. Getautis, S. Albrecht, Science 2020, 370, 1300.

[12] M. Jošt, L. Kegelmann, L. Korte, S. Albrecht, Advanced Energy Materials 2020, 10, 1904102.

[13] X. He, J. Chen, X. Ren, L. Zhang, Y. Liu, J. Feng, J. Fang, K. Zhao, S. Liu, Advanced Materials 2021, 33, 2100770.

[14] D. Lübke, P. Hartnagel, J. Angona, T. Kirchartz, Advanced Energy Materials 2021, 11, 2101474.

[15] O. Almora, D. Baran, G. C. Bazan, C. I. Cabrera, S. Erten-Ela, K. Forberich, F. Guo, J. Hauch, A. W. Y. Ho-Baillie, T. J. Jacobsson, R. A. J. Janssen, T. Kirchartz, N. Kopidakis, M. A. Loi, R. R. Lunt, X. Mathew, M. D. McGehee, J. Min, D. B. Mitzi, M. K. Nazeeruddin, J.

Nelson, A. F. Nogueira, U. W. Paetzold, B. P. Rand, U. Rau, H. J. Snaith, E. Unger, L. Vaillant-Roca, C. Yang, H.-L. Yip, C. J. Brabec, Advanced Energy Materials 2023, n/a, 2203313.

[16] E. T. Hoke, D. J. Slotcavage, E. R. Dohner, A. R. Bowring, H. I. Karunadasa, M. D. McGehee, Chemical Science 2015, 6, 613.

[17] E. L. Unger, L. Kegelmann, K. Suchan, D. Sorell, L. Korte, S. Albrecht, Journal of Materials Chemistry A 2017, 5, 11401.

[18] S. Mahesh, J. M. Ball, R. D. Oliver, D. P. McMeekin, P. K. Nayak, M. B. Johnston, H. J. Snaith, Energy & Environmental Science 2020, 13, 258.

[19] Z. Liu, J. Siekmann, B. Klingebiel, U. Rau, T. Kirchartz, Advanced Energy Materials 2021, 11, 2003386.

[20] J. Tian, K. Zhang, Z. Xie, Z. Peng, J. Zhang, A. Osvet, L. Lüer, T. Kirchartz, U. Rau, N. Li, C. J. Brabec, ACS Energy Letters 2022, 7, 4071.

[21] H. Chen, A. Maxwell, C. Li, S. Teale, B. Chen, T. Zhu, E. Ugur, G. Harrison, L. Grater, J. Wang, Z. Wang, L. Zeng, S. M. Park, L. Chen, P. Serles, R. A. Awni, B. Subedi, X. Zheng, C. Xiao, N. J. Podraza, T. Filleter, C. Liu, Y. Yang, J. M. Luther, S. De Wolf, M. G. Kanatzidis, Y. Yan, E. H. Sargent, Nature 2022.

[22] M. Stolterfoht, P. Caprioglio, C. M. Wolff, J. A. Márquez, J. Nordmann, S. Zhang, D. Rothhardt, U. Hörmann, Y. Amir, A. Redinger, Energy & Environmental Science 2019, 12, 2778.

[23] S. N. Agbo, T. Merdzhanova, U. Rau, O. Astakhov, Solar Energy Materials and Solar Cells 2017, 159, 427.

[24] F. Khan, S. N. Singh, M. Husain, Sol Energ Mat Sol C 2010, 94, 1473.

[25] N. H. Reich, W. G. J. H. M. van Sark, E. A. Alsema, R. W. Lof, R. E. I. Schropp, W. C. Sinke, W. C. Turkenburg, Sol Energ Mat Sol C 2009, 93, 1471.

[26] J. Merten, J. M. Asensi, C. Voz, A. V. Shah, R. Platz, J. Andreu, IEEE Transactions on Electron Devices 1998, 45, 423.

[27] G. Burwell, O. J. Sandberg, W. Li, P. Meredith, M. Carnie, A. Armin, Solar RRL 2022, 6, 2200315.

[28] R. Arai, S. Furukawa, Y. Hidaka, H. Komiyama, T. Yasuda, ACS Applied Materials & Interfaces 2019, 11, 9259.

[29] R. Cheng, C.-C. Chung, H. Zhang, F. Liu, W.-T. Wang, Z. Zhou, S. Wang, A. B. Djurišić, S.-P. Feng, Advanced Energy Materials 2019, 9, 1901980.

[30] J. Dagar, S. Castro-Hermosa, G. Lucarelli, F. Cacialli, T. M. Brown, Nano Energy 2018, 49, 290.

[31] C.-Y. Chen, J.-H. Chang, K.-M. Chiang, H.-L. Lin, S.-Y. Hsiao, H.-W. Lin, Advanced Functional Materials 2015, 25, 7064.

[32] L.-C. Kin, Z. Liu, O. Astakhov, S. Shcherbachenko, H. Kungl, T. Kirchartz, R.-A. Eichel, U. Rau, T. Merdzhanova, Cell Reports Physical Science 2022, 3, 101123.

[33] V. Bahrami-Yekta, T. Tiedje, Opt Express 2018, 26, 28238.

[34] Z. Liu, L. Krückemeier, B. Krogmeier, B. Klingebiel, J. A. Márquez, S. Levcenko, S. Öz, S. Mathur, U. Rau, T. Unold, T. Kirchartz, ACS Energy Letters 2019, 4, 110.

[35] M. A. Faist, S. Shoaee, S. M. Tuladhar, G. F. A. Dibb, S. Foster, W. Gong, T. Kirchartz, D. D. C. Bradley, J. R. Durrant, J. Nelson, Advanced Energy Materials 2013, 3, 744.

[36] M. A. Faist, T. Kirchartz, W. Gong, R. S. Ashraf, I. McCulloch, J. C. de Mello, N. J. Ekins-Daukes, D. D. C. Bradley, J. Nelson, Journal of the American Chemical Society 2012, 134, 685.

[37] L. Krückemeier, Z. Liu, B. Krogmeier, U. Rau, T. Kirchartz, Advanced Energy Materials 2021, 11, 2102290.

[38] M. A. Green, U. o. N. S. Wales, *Solar Cells: Operating Principles, Technology and System Applications*, University of New South Wales, 1986.

[39] S. Hegedus, A. Luque, *Handbook of Photovoltaic Science and Engineering*, Wiley, 2011.

[40] M. A. Green, Solar cells 1982, 7, 337.

[41] S. Agbo, T. Merdzhanova, U. Rau, O. Astakhov, Sol Energ Mat Sol C 2017, 159, 427.

[42] J. Merten, J. Asensi, C. Voz, A. Shah, R. Platz, J. Andreu, IEEE Transactions on electron devices 1998, 45, 423.

[43] L. C. Hirst, N. J. Ekins-Daukes, Progress in Photovoltaics: Research and Applications 2011, 19, 286.

[44] D. Grabowski, Z. Liu, G. Schöpe, U. Rau, T. Kirchartz, Solar RRL 2022, 6, 2200507.

[45] D. Lübke, P. Hartnagel, M. Hülsbeck, T. Kirchartz, ACS Materials Au 2023, 3, 215.

[46] M. Taguchi, A. Yano, S. Tohoda, K. Matsuyama, Y. Nakamura, T. Nishiwaki, K. Fujita, E. Maruyama, Ieee J Photovolt 2014, 4, 96.

[47] S. K. Thomas, A. Pockett, K. Seunarine, M. Spence, D. Raptis, S. Meroni, T. Watson, M. Jones, M. J. Carnie, IoT 2022, 3, 109.

[48] X. Deng, X. Wen, J. Zheng, T. Young, C. F. J. Lau, J. Kim, M. Green, S. Huang, A. Ho-Baillie, Nano Energy 2018, 46, 356.

[49] S. Shao, M. Abdu-Aguye, L. Qiu, L.-H. Lai, J. Liu, S. Adjokatse, F. Jahani, M. E. Kamminga, H. Gert, T. T. Palstra, Energy & environmental science 2016, 9, 2444.